DEUTSCHES ELEKTRONEN-SYNCHROTRON DESY

DESY 84-122
December 1984

THE TOTAL CROSS SECTION $\gamma\gamma \to$ HADRONS

by

G. Knies

Deutsches Elektronen-Synchrotron DESY, Hamburg

ISSN 0418-9833

NOTKESTRASSE 85 · 2 HAMBURG 52

To be sure that your preprints are promptly included in the
HIGH ENERGY PHYSICS INDEX ,
send them to the following address (if possible by air mail) :

DESY
Bibliothek
Notkestrasse 85
2 Hamburg 52
Germany

DESY 84-122
December 1984

ISSN 0418-9833

THE TOTAL CROSS SECTION $\gamma\gamma \to$ HADRONS

Gerhard Knies

DESY
2000 Hamburg 52
Germany

ABSTRACT

Measurements of the total cross section for $\gamma\gamma \to$ hadrons are presented. There are new results from double-tagging ($P^2 \neq 0$, $Q^2 \neq 0$, single-tagging ($P^2 \approx 0$, $Q^2 \neq 0$), and no-tagging ($P^2 \approx 0$, $Q^2 \approx 0$) experiments at e^+e^- storage rings. The measurements cover a Q^2 range from 0 to 100 GeV^2, and a W range from 2 to 20 GeV. The significance of these data for the interpretation of the photon as a set of vector mesons (VDM) and as an electromagnetic field quantum coupling to point-like quarks (QPM) is discussed.

OUTLINE:

1. Introduction

Much has already been said about the total cross section $\sigma^{tot}(W, Q^2 = -\gamma_1^2, P^2 = -\gamma_2^2)$ for

$$\gamma_1\gamma_2 \to \text{hadrons}$$

in the two preceeding talks[1,2] in terms of the hadronic structure function F_2^{had} of the photon, via the relation

$$\sigma^{tot}(W, Q^2 \gg 0, P^2 \approx 0) = \sigma_{TT} + \sigma_{LT} = \frac{4\pi^2\alpha}{Q^2} F_2^{had}\left(x = \frac{Q^2}{Q^2+W^2}, Q^2\right) \quad (1)$$

Has all been said?

No, since firstly in the kinematic region ($P^2 > 0$, $Q^2 > 0$), that is for double-tag data relation (1) is no longer a valid approximation. The total cross section here has the form[3] (see section 3 for definitions and Fig. 1 for notations):

$$\sigma^{tot} = \sigma_{TT} + \sigma_{LT} + \sigma_{TL} + \sigma_{LL} \quad (2)$$

while the structure function F_2 is related[4] to the cross section by

$$F_2(x,Q^2,P^2) = \frac{Q^2}{4\pi^2\alpha}(1-Q^2P^2\nu^2)^{-1/2}\{\sigma_{TT} + \sigma_{LT} - \frac{1}{2}\sigma_{TL} - \frac{1}{2}\sigma_{LL}\} \quad (3)$$

Secondly, for $Q^2 \ll 1$ GeV^2 and - as always - $P^2 < Q^2$, relation (1) becomes useless, since the predictions for F_2^{had} become meaningless. The reason is that QCD predictions for F_2^{had} are based on perturbative calculations of the photon splitting process[5]:

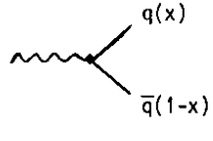

and on a probabilistic interpretation of q(x) as the quark distribu-

tion function:

$$F_2(x) = x \cdot q(x) \qquad (4)$$

Since this $q^{QCD}(x)$ is proportional to $\ell n\, Q^2/\Lambda^2$, it turns negative for $Q^2 < \Lambda^2$, in obvious conflict with the probabilistic interpretation. Heuristically this means that for $Q^2 \lesssim \Lambda^2$ the probing photon no longer resolves in space the virtual quark states, to an extent that incoherent interaction of the quark and antiquark with the probing photon becomes impossible. However, the total cross section remains a meaningful physics quantity also at $Q^2 \to 0$.

Previous measurements of the total $\gamma\gamma$ cross section[6] at low Q^2 ($Q^2 \lesssim 1$ GeV) are largely in agreement with the VDM expectation[7] for virtual vector meson vector meson collisions and are much larger than predicted by the (perturbative) calculation in the quark parton model (QPM). At high Q^2 ($Q^2 \gtrsim 20$ GeV^2) the cross section predicted through perturbative F_2^{had} calculations[7] accounts approximately for the measured total cross section. The notion of a cross section is therefore more useful than that of a structure function in studying the transition of the photon from a set of vector mesons to an electromagnetic field quantum with point-like couplings to quarks, since there are predictions in the full Q^2 region.

In this talk I will present and discuss results on cross section measurements in double-tag experiments ($P^2 > 0$), and from no-tag and single-tag experiments with $P^2 \approx 0$ and Q^2 from ≈ 0 to ≈ 100 GeV^2. In the latter case, the evolution of σ^{tot} with Q^2 allows us to study the interplay of the vector mesonic and point-like nature of the photons.

2. Predictions for $\sigma^{tot}_{\gamma\gamma}(W, Q^2, P^2)$

There are two extreme types of predictions, corresponding to treating the photon as an electromagnetic field quantum interacting

with the charge of point-like quarks:

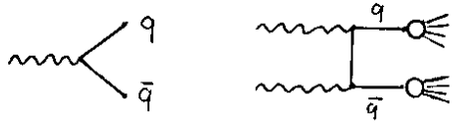

or replacing the photon by a hadronic current, saturated by vector mesons:

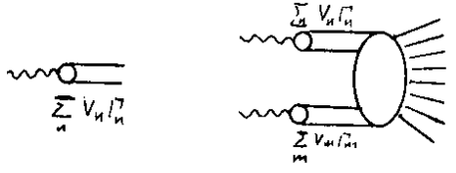

In the first approach $\sigma(W, Q^2, P^2)$ can be evaluated in terms of the QPM[3] if all gluon radiation corrections are ignored, by introducing quark masses and charges as the only unknown parameters. In the VDM approach, in the decomposition of the hadronic current into vector mesons, the vector meson masses m_V, the γ-V couplings and the cross section $\sigma^{tot}(VV')$ have to be specified.

As long as full QCD calculation for $\gamma\gamma \to$ hadrons is not available it is of interest how these two approaches can be combined.

2.1 Brief review of experimental facts in support of the point-like and of the VDM hadronic nature of the photon

a) Q^2 time-like: here the total cross section $\sigma(e^+e^- \to \gamma \to \text{hadrons})$ gives support for either picture, as alternatives:
at $Q^2 \approx m^2_{\rho,\omega,\phi}$: γ like VDM
at $Q^2 \gg m^2_\rho$: γ couples to point-like quarks in the QPM approximation

b) $Q^2 = 0$: Measurements on $\frac{d\sigma}{dt}(\gamma N \to N + \rho,\omega,\phi)$ and σ_{tot} ($\gamma p \to$ hadrons) confirmed the Vector Dominance Model (VDM) in a quantitative way.

c) Q^2 space like: The deep inelastic inclusive ep scattering experiments i.e. $\gamma^* p \to$ hadrons lead to the introduction of the Quark Parton Model (QPM)[9].

2.2 Duality and double counting

However, it was also possible to describe or parametrize the deep inelastic ep data in terms of a Generalized (GVDM)[10] or Extended Vector Dominance Model (EVDM)[11], and it was even claimed that the Q^2 dependence did arise from heavy vector meson states. These models also described $\sigma^{tot}(e^+e^- \to \gamma \to \text{hadrons})$ at $-Q^2 = s \gg m_\rho^2$, and in the resonance region.

It was obvious that the QPM and the (E or G) VDM parametrizations should not be added, under these circumstances. Sakurai[8] therefore proposed a new duality which is expressed in the following FESR:

$$\int_{4m_\pi^2}^{S_{max}} s \cdot \sigma(e^+e^- \to \gamma^* = \sum_n V_n \cdot \Gamma_n \to \text{hadrons})\, ds = \int_{S_0}^{S_{max}} s \cdot (e^+e^- \to \gamma^* = \sum_q q\bar{q} \cdot \alpha_q \to \text{hadrons})\, ds \qquad (5)$$

It says that the VDM hadronic and the point-like picture of the photon are equivalent on average. Therefore the combination of both:

$$\sigma^{tot}(e^+e^- \to \text{had}) = \sigma(\text{QPM}) + \sigma((\text{G,E})\text{VDM}) \qquad (6)$$

is double counting in this picture.

2.3 Is eγ like ep?

Since ep scattering is well described by the VDM approaches eγ scattering may be as well. In fact if the transition of a photon into hadrons can be fully described by a coupling of the photon to an infinite set of (extended) vector mesons V_n, with an appropriate choice of couplings Γ_n and masses m_n, then eγ scattering can be linked to ep in the following way:

$$\sigma^{tot}(\gamma^* p) = \sigma^{tot}((\sum_n \Gamma_n V_n)p) \qquad (7a)$$

$$\sigma^{tot}(\gamma^* \gamma) = \sigma^{tot}((\sum_n \Gamma_n V_n)(\sum \Gamma_m V_m) \qquad (7b)$$

Relating the (virtual) vector meson proton cross section $\sigma(V_n P)$ to $\sigma(V_n V_m)$ allows then to predict $\sigma(e\gamma)$ from $\sigma(ep)$.

In ep scattering, the target is an extended hadron, however, and therefore the VDM parametrization of the probing photon may be appropriate to describe the Q^2 dependence of the ep cross section. In eγ scattering the target is not necessarily an extended hadron. Therefore, VDM parametrizations of the target and probing photons may not be appropriate. Furthermore, EVDM, GVDM and QPM predict different Q^2 dependences of $\sigma_{\gamma\gamma}^{tot}$ on average. So these approaches cannot be equivalent here in a dual sense. The W dependences of $\sigma(W, Q^2, P^2 \approx 0)$ differ as well, since the QPM predicts no W independent term at small Q^2, but the EVDM does. A measurement of the W and Q^2 dependences of $\sigma_{\gamma\gamma}^{tot}(W, Q^2)$ is therefore suitable to study the roles of the point-like and the VDM nature of the photon.

3. What can be measured in $e^+e^- \to e^+e^-$ + hadrons?

Using the notation of Fig. (1) and following ref. 3 we here briefly summarize the most important cross section expressions for the reaction

$$e^+e^- \to e^+e^- + \text{hadrons} \qquad (8)$$

3.1 Double-tag mode

$$d\sigma_{ee} = \{\Gamma_{TT} \cdot \sigma^{eff} + \frac{1}{2}\varepsilon_1\varepsilon_2\tau_{TT} \cdot \cos 2\phi + 2\sqrt{\varepsilon_1(\varepsilon_1+1)\varepsilon_2(\varepsilon_2+1)}\,\tau_{TL}\cos\phi\}\,\frac{d^3p_1}{E_1}\cdot\frac{d^3p_2}{E_2} \quad (9)$$

with $\sigma^{eff} = \sigma_{TT} + \varepsilon_2 \cdot \sigma_{TL} + \varepsilon_1\sigma_{LT} + \varepsilon_1\varepsilon_2\sigma_{LL}$ (10)

σ and τ are $\gamma\gamma$ cross sections and interference terms, T,L indicate transverse and longitudinal photons

$$\sigma_{TT} = \frac{1}{2}(\sigma_{\parallel} + \sigma_{\perp}) = \frac{1}{2}(\sigma_0 + \sigma_2) \quad (11)$$

$$\tau_{TT} = \sigma_{\parallel} - \sigma_{\perp} \quad (12)$$

with $\sigma_{\parallel}$ and $\sigma_{\perp}$ (σ_0 and σ_2) the cross sections for scattering of transverse photons with parallel and perpendicular linear polarization (with helicity 0 and helicity 2). Gauge invariance implies for $q_i^2 \to 0$

$$\sigma_{TL} \sim q_2^2,\ \sigma_{LT} \sim q_1^2,\ \sigma_{LL} \sim q_1^2q_2^2,\ \tau_{TL} \sim \sqrt{q_1^2q_2^2} \quad (13)$$

Γ_{TT} is the flux factor for the transverse photons at vertex 1 and 2.
Γ_{LT} is the flux factor for longitudinal photons at vertex 1.
$\varepsilon_1 = \Gamma_{LT}/\Gamma_{TT}$, $\varepsilon_2 = \Gamma_{TL}/\Gamma_{TT}$ are the polarization parameters.

ϕ is the angle between the electron and positron scattering planes in the $\gamma\gamma$ CMS.

In double tag experiments σ^{eff}, τ_{TT} and τ_{TL} can be measured.

3.2 Single tag mode

Averaging over ψ_2, the azimuthal angle of e_2, and $-q_2^2 = P^2 \approx 0$ lead to $\sigma_{TL} = 0$, $\sigma_{LL} = 0$, $\tau_{TL} = 0$, and $\langle\cos 2\phi\rangle = 0$, which simplifies expressions (9) and (10) for reaction (8):

$$d\sigma_{ee} = \frac{\alpha\cdot E_1\cdot(1+(1-y)^2)}{2\pi^2Q^2y}\ \{\sigma^{tot} + (\varepsilon_2-1)\cdot\sigma_{TL}\}\cdot N_{\gamma}(z_2,\theta_2^{max})\,dz_2\,dE_1\,d\Omega_1 \quad (14)$$

with $\sigma^{tot} = \sigma_{TT} + \sigma_{TL}$.

$N(z_2,\theta_2^{max})$ describes the flux of quasireal target photons[3] of fractional energy $z_2 = E_2^{\gamma}/E_b$ with emission angles smaller than θ_2^{max}:

$$N_{\gamma}(z,\theta^{max}) = \frac{\alpha}{\pi}\cdot\frac{1}{z}\{1+(1-z)^2)\ln\frac{E_b(1-z)\theta^{max}}{m_e z} - (1-z)\} \quad (15)$$

y is determined from the tagged electron $y = 1-(E_1/E_b)\cdot\cos^2(\theta_1/2)$.
In the actual experiments the tag energy and angle constraints make $\varepsilon_2 \sim 1$ so that the σ_{TL} term in (14) can be neglected.

3.3 No tag mode

The double anti-tagging leads to $P^2 = Q^2 \approx 0$, and eq. (14) reduces to

$$d\sigma_{ee} = \sigma_{TT}(W)\ \ N(z_2,\theta_2^{max})\,N(n_1,\theta_1^{max})\ dz_2dz_1 \quad (16)$$

4. Experiments

Since the last $\gamma\gamma$ workshop[12] in 1983 there is a substantial improvement of data. Table I gives a summary on the new experimental data.

Table I

Summary on experiments with new results presented to this workshop.

Tagging Mode	Experiment	P^2, Q^2 $(GeV)^2$	E_b GeV	Luminosity nb^{-1}	Events
No tag = double antitag	PLUTO	$P^2=Q^2\approx.01$	17.3	4.8	5223
Single tag $P^2\approx.01$	PLUTO	Q^2 0.1 - 0.9	17.3	19	2931
		1.1 - 20	17.3	37	1587
		15 - 130	17.3	40	105
Double tag	PEP 4/9	P^2, Q^2 0.1 - 1.6	14.5	50	790

4.1 Experimental setups

Figs. 2a and 2b show the salient features of the PLUTO and the PEP4/9 detectors. The PEP4/9 results are derived from double tag events using the NaI shower counters, and the PLUTO results are derived from no-tag and single-tag data using the small and large angle taggers (SAT and LAT, respectively), and the end cap shower counters (ECT). Table II summarizes the relevant properties of the tagging systems.

Table II

Properties of tagging systems

Experiment	P L U T O			PEP4/9
tagger	SAT	LAT	EC	NaI
polar angle	32-55	90-260	330-680	22-90 mrad
azimuthal angle ψ	2π	180 ± 65 ~~0 ± 65~~	2π	2π
tagging energy resolution $\Delta E/\sqrt{E}$	16.5%	25%	28%	$\frac{\Delta E}{E}$ = 1% at 14.5 GeV
tagging energy trigger threshold	E > 4	E > 4	E > 3	E_1, E_2 > 0.8 GeV
other trigger requirements	≥ 1 track in central detector	none	none	$\lvert\psi_1-\psi_2\rvert$ > 0.3 (>0.55 off line)
Q^2-range (GeV^2)	.14 -.91	1.1-20	15-130	$0.1 < Q^2, P^2 < 1.6$

4.2 Background rejection

The rejection of background is a major task before cross sections can be inferred from triggered events. The contamination of $\gamma\gamma$ events by other sources is the more severe the less tags are required: the no-tag data are heavily contaminated and the double tag data are almost clean. The separation of the channels $\gamma\gamma \to$ leptons and $\gamma\gamma \to$ hadrons requires further cuts. Table III shows a survey of

the relevant background sources, together with the most efficient cuts for their remedy.

Table III

Survey on background sources for $\gamma\gamma \to$ hadrons

Source		Remedy
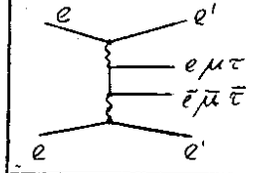	$\gamma\gamma$ events, but 'QED'	2prg + $\geq$ 1 shower, or $\geq$ 3prg remaining $\tau\bar{\tau}$ subtracted
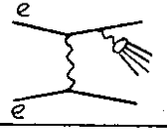	'inelastic' compton	$W_{vis} \gtrsim$ 1 GeV
$eN \to e'$ + had	beam gas	$W_{vis} \geq$ 1 GeV tracks with negative charge, side band subtraction
$e^+e^- \to$ hadrons 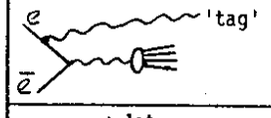 'tag'	radiative annihilation	tagging track $W_{vis} \lesssim$ 10 GeV $n_{ch} \lesssim 10$
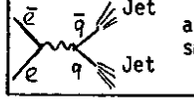 Jet at small θ Jet	jet into tagging system	"Isolated" tag p^{miss} cut

In table IV we summarize the cuts applied to the no-tag, single-tag and double-tag samples, respectively, and the remaining background contents.

TABLE IV

Final state cuts which limit the acceptance

Quantity	no-tag	single-tag	double-tag
Anti-tag	$\theta_1, \theta_2 > 30$ mrad $E_1, E_2 > 4$ GeV	$\theta_1 > 30$ mrad $E_1 > 4$ GeV	-
Multiplicity	$3 \leq N_{CH} \leq 10$ at $\theta > 30^o$ not all same charge sign	N_{CH}=2, + $\geq$1 sh. $N_{CH} \geq 3$ 1 track+electr. for N_{CH} = 2,3	N_{CH}=2, + $\geq$ 1 sh. $N_{CH} \geq 3$ 1 track+electr for N_{CH} = 2,3
W_{vis}	$1.5 < W_{vis} < 10$	$1.2 < W_{vis} < 10$	
net longitudinal momentum		$\lvert p_2^{miss} \rvert > 6$ GeV opp. to tagged electron	

Resulting events and background

Events	no tag 5223	SAT 2931	LAT 1587	ECT 105	double tag ~790
Background%					
$\gamma\gamma \to \tau\tau$	1	1.5	5	10	< 5
beam gas	6	4	4	-	-
annihilation	8	-	< 1	9	-

For the no-tag data the background situation is illustrated in Fig. 3. Fig. 3a shows the observed W_{vis} distribution of the no-tag events in the full W_{vis} range. At $W_{vis} < 10$ GeV a clear enhancement due to $\gamma\gamma$ events is seen. At an expanded scale, the data at $W_{vis} < 10$ GeV are compared in Fig. 3b to the sum of the $\gamma\gamma$ MC prediction using the $\sigma_{\gamma\gamma}(W)$ as resulting from the unfolding, the $\gamma\gamma \to \tau\tau$ and e^+e^- annihilation contamination as estimated by MC simulation, and the beam gas event contribution. The observed W_{vis} distribution is well reproduced by the resulting $\sigma_{\gamma\gamma}(W)$ and the estimated background contributions. Fig. 3c shows the share of the contaminations relative to the total. The W_{vis} region above 9 GeV is too much contaminated for a reliable $\gamma\gamma$ cross section determination.

5. Determination of cross section

To evaluate cross sections from the data one has to deal with 3 further problems:

i) the Q^2 (P^2) interpolation
ii) the $W_{vis} \to W$ correction
iii) and acceptance corrections

5.1 The Q^2 (P^2) interpolation

The single- and double-tagged data cover Q^2 and P^2 ranges over which $\sigma(W,Q^2,P^2)$ varies by orders of magnitude. Since event statistics is limited a real multidimensional cross section analysis is not possible, however. Therefore, within limited Q^2 regions (see Table V) factorization is assumed in evaluating $\sigma(W, \langle Q^2\rangle, \langle P^2\rangle)$ in these intervals from $\sigma(W,Q^2,P^2)$:

$$\sigma(W, \langle Q^2\rangle, \langle P^2\rangle) = \sigma(W, Q^2, P^2) \cdot \frac{F(\langle Q^2\rangle)}{F(Q^2)} \cdot \frac{F(\langle P^2\rangle)}{F(P^2)} \qquad (17)$$

The interpolation functions $F(Q^2)$ given in Table V have been checked to describe the data (see Figs. 4a,b for the GVDM form factor).

Table V

Intervals in tagged data, and Q^2 interpolation functions

Tagger	SAT	LAT	ECT	NaI
Q^2 range	.14 - .91	1.1 - 20	15 - 130	$1 < P^2, Q^2 < 1.6$
$\langle Q^2\rangle$	.44	5.4	45	0.3
$F(Q^2)$	GVDM	$Q^{-0.9}$	$Q^{-0.9}$	GVDM

5.2 W_{vis} correction

In the no-tag and single-tag data, the effective mass W_{vis} of the observed final state particles is measured instead of the effective mass W of the $\gamma\gamma$ system. In the PLUTO experiment W_{vis} is near 75% of W on average, with a spread of about 25%. Fig. 5 shows the W_{vis}/W ratio for simulated events tagged in the SAT. The original W distribution is reconstructed using the $W - W_{vis}$ correlation from simulated events (see section 5.4), and an unfolding procedure.

In double-tag experiments W is calculated from the colliding photon energies directly:

$$W^2 = 4E_1^\gamma E_2^\gamma - 2E_1^\gamma E_2^\gamma \sin\theta_1 \sin\theta_2 \cdot \sin\phi/2 \qquad (18)$$

At low W (< 3 GeV), however, the resolution is rather poor $\sigma(W) \sim 0.8$ GeV, and initial state radiation pushes W below the true W value. The measured double-tag W distribution (Fig. 6a) has been

corrected for these effects (Fig. 6b). At W < 4 GeV the corrected distribution is considerably different from the measured one.

5.3 Acceptance corrections

The detection efficiencies for the final state of tagged events is limited because of the cuts described in section 4. Fig. 7 shows as examples the acceptance as function of W, for the PLUTO SAT and for the PEP4/9 double-tagged events. Acceptance corrections are small, very little model dependent and pretty similar in both experiments at W > 5 GeV. At lower W values, the PEP4/9 double-tagged data have a considerably larger acceptance than the PLUTO SAT data. The acceptance values here depend more on the details of the final state model, in particular on the charged multiplicities.

5.4 Hadronic final state model

The unfolding procedure requires the use of simulated events for the reaction $\gamma\gamma \to$ hadrons. To generate such events a model for hadronization is required. The PEP4/9[13] and the PLUTO[14-16] analysis used the models summarized in Table VI. At the low W end (W < 4 GeV), the charged multiplicity pattern is particularly important for the event acceptance calculations. The average multiplicities for charged and neutral pions differ in the two analyses. The PLUTO analysis uses a multiplicity parametrization which is close to the e^+e^- annihilation data[17] in that energy range (Fig. 8), while the PEP4/9 parametrization is substantially below the e^+e^- data at W < 7 GeV. Both experiments claim they reproduce their observed multiplicities well. There is, however, no evidence presented that the PEP4/9 data are inconsistent with the e^+e^- average together with a KNO distribution.

Table VI

Parametrization of the hadronic final state models

Particles	PLUTO	PEP4/9
Multiplicity		
Average		
$\langle\pi^+ + \pi^-\rangle$	$2 \cdot \sqrt{W}$	$1 + 0.52W$ (GeV)
$\frac{\langle\pi^0\rangle}{\langle\pi^+ + \pi^-\rangle}$	$\frac{2}{3}$	$\frac{1}{2}$
Distribution	KNO	Poisson
	$\frac{\langle N\rangle}{D} = 2.7\ \pi^\pm$ $2.4\ \pi^0$	
Topology:		
a) invariant phase space (IP)		
b) limited $p_\perp$ phase space (LP)		
	$LP = IP * \prod_{i=1}^{N} \exp\{-5p_\perp^2\}$	$LP = IP * \prod_{i=1}^{N} \exp\{-6.25p_\perp^2\}$
c) $\gamma\gamma \to q\bar{q}$ with QED angular distribution (QM)		

A possible bias of this difference on the acceptance correction should go in the direction that it was estimated too small in the PLUTO and/or too large in the PEP4/9 analysis, relatively. The different multiplicity parametrizations may introduce a systematic difference between the two $\sigma(W)$ evaluations at low W.

There is a further difference in so far as in the PLUTO analysis also the rejected $\pi^+\pi^-$ and $\pi^0\pi^0$ final states have been corrected for. They contribute, however, only 0.6% to σ^{tot} at W = 2 GeV according to the model, a number which is confirmed by a direct mesurement of the exclusive reaction $\gamma\gamma \to \pi^+\pi^-$ [18].

To achieve a good reproduction of their data the PLUTO collaboration had to use a W depending mixture of different topological models (see Table V), with IP topology dominating at low W ($\lesssim$ 4 GeV) and $P_\perp$ limited topologies (LP, QM) dominating at W $\gtrsim$ 7 GeV.

5.5 The unfolding procedure

With the definition of a model for $\gamma\gamma \to$ hadrons, where $\sigma(W)$ is not jet fixed, an unfolding procedure[19] can be applied to search for a smooth function $\sigma(W)$ which reproduces the observed W_{vis} distribution. The unfolding method applied by the PLUTO collaboration has been described in detail at this workshop[20].

By including the experimental luminosity, a full detector simulation for the events and the Q^2 interpolating functions (see Table V) the resulting cross section $\sigma(W)$ is

a) interpolated to $Q^2 = \langle Q^2 \rangle$
b) corrected for all event acceptance inefficiencies
c) unfolded for the $W \to W_{vis}$ transition due to resolution and particle losses.

Two types of checks on the reliability of the unfolding step have been performed. The first check concerns the reliability of the estimate of the amount of unobserved or rejected events. This number depends mainly on a correct estimate of events with low observed multiplicity ($N_{CH} \leq 2$) in the simulation model. Fig. 8(b and c) checks how well the observed charged multiplicity is reproduced, and Fig. 9 checks the charged particles momenta transverse to the e^+e^- beam, since low $p_\perp$ ($p_\perp \lesssim 0.1$ GeV) tracks are not detected with full efficiency. There is no obvious mismatch between the data and their simulation, except for the $P_\perp^2$ distribution of PEP4/9 at $p_\perp^2 > 0.4$ GeV^2 reflecting the exclusive use of a limited $p_\perp$ model. The authors claim, however, that the acceptance efficiency is insensitive to this $p_\perp$ region.

The second check concerns the reliability of the $W_{vis} \to W$ unfolding. To this end the PLUTO collaboration applied the unfolding procedure to a simulated ee → ee + hadrons experiment. Fig. 10 shows the "true" cross section $\sigma(W)$ as a curve, and the reconstructed cross section as a histogram. For W > 2 GeV the reconstruction is perfect. Only the steep slope of a $1/W^2$ term below W = 2 GeV in Fig. 10b is marginally recovered.

6. Results on σ^{tot} ($\gamma\gamma \to$ hadrons)

The total cross section results $\sigma(W, \langle Q^2 \rangle, \langle P^2 \rangle)$ are shown in Fig. 11. This figure shows the W-dependence of σ from no-tagging, single-tagging and double-tagging measurements, together with their respective average Q^2 and P^2 values. The Q^2 dependence, $\sigma(\langle W \rangle, Q^2)$, for σ averaged over the W interval $3 < W < 10$ GeV from single-tagging data is shown in Fig. 12. In Fig. 13 the double-tagging cross section in ϕ intervals averaged over the full W(2-20 GeV) and q_i^2 (0.1 - 1.6 GeV^2) regions is given. Fig. 11 - 13 contain all results of the $\gamma\gamma$ total cross section measurements. What do they tell us?

6.1 Analysis of the ϕ dependence

A fit of (9) to Fig. 13 yields the following results

$$\tau_{TT}/\sigma^{eff} = -0.43 \pm 0.23 \qquad (19a)$$

$$\tau_{LT}/\sigma^{eff} = -0.01 \pm 0.03 \qquad (19b)$$

The latter one is expected because of (13), and the first one indicates $\sigma_\perp \geq \sigma_{||}$ (see (12)).

6.2 W-dependence of σ^{tot} at different P^2 and Q^2 values

Here are two points of interest:

1. Does $\sigma(W, Q^2, P^2)$ factorize, as expressed in (17)?
2. Which W^n terms are present in $\sigma(W)$?

By comparing the no-tag and the SAT single-tag ($\langle Q^2 \rangle$ = 0.44 GeV) cross sections with the other ones of Fig. 11, it is obvious that W-Q^2-P^2 factorization of σ^{tot} does not work. Even though the SAT and the double-tagging data have about the same level of cross section, i.e. the same amount of suppression as compared to $P^2 = Q^2 = 0$, their W-dependences are clearly different. A potential inconsistency in the data analysis from the different multiplicity parametrizations employed (see section 5.4) might even work into the direction opposite to the observed differences. The other difference between the two experiments is the method to determine W. Whether this difference leads to a systematic difference in σ^{tot} at low W might be checked with the PEP4/9 data which allow to use the single-tagging method - W from unfolding of W_{vis} as calculated from the observed hadrons - in addition to the double-tagging method of eq. (18).

With the data as presented we have to conclude that $\sigma(W, \langle Q^2 \rangle = 0.44, P^2 = 0)$ cannot be converted into $\sigma(W, \langle Q^2 \rangle = \langle P^2 \rangle = 0.3\ \text{GeV}^2)$ by

a factorizing ansatz (Fig. 15). This is even more surprising when looking at Fig. 4. Both experiments demonstrate that for their rather wide regions of Q^2 - wide as compared to the differences between the two experiments, where Q^2_{max} from double-tagging and Q^2 from single-tagging overlap largely - factorization with the GVDM form factor is consistent with their data, since low and high W data scale alike.

The decomposition of $\sigma(W, \langle Q^2 \rangle)$ into terms of W^0, $1/W$ and $1/W^2$ is of interest from a t-channel or Regge point of view. The presently available data suffer from rather large systematic errors (> 20%) at small W (< 4 GeV) making a meaningful determination of terms with different powers in W practically impossible. All one can say is that only the PLUTO SAT data establish a declining cross section with growing W. It can be fitted (see Fig. 14) to shapes like

$$\sigma(W) = (107 \pm 40) + \frac{933 \pm 112}{W} \ [\text{GeV, nb}] \qquad (20a)$$

$$\text{or} \quad = (0.91 \pm 0.08)\ (240 + \frac{270}{W}) + \frac{941 \pm 186}{W^2} \ [\text{GeV, nb}] \qquad (20b)$$

after GVDM extrapolation to $Q^2 = 0$. The W dependent fraction is stronger than in the traditional[21] 240 + 270/W parametrization. Because of (20a) the necessity of a $1/W^2$ term, however, is not established. The no-tag cross section has too short a leaver arm in W and too large systematic errors for any conclusion. The double-tag cross section is constant between 2 and 20 GeV ($\sigma = (380 \pm 60) + (70 \pm 290)/W$) and the single-tag cross sections at $\langle Q^2 \rangle$ = 5.4 and 45 GeV^2 are consistent with constant, but have rather large errors.

6.3 Point-like and hadron-like behaviour of the photon

The point we want to investigate here is not whether the point-like cross section contribution of the photon as predicted by QED and the QPM exists. It has been clearly observed in the jet analysis of $\gamma\gamma \to$ hadrons[22] and has been discussed in previous talks[2,23] at this workshop.

Nor is the point whether VDM type contribution exist in $\gamma\gamma \to$ hadrons. Again the jet analysis[22,23] demonstrates that - beyond the size of the total $\gamma\gamma$ cross section at low Q^2 - also topological properties of the hadronic final state require VDM type contributions.

The point of concern is how these two pictures of the photon have to be combined in order to describe the facts. For this question the total $\gamma\gamma$ cross section is supplementary to the jet analysis. Firstly because also data at $W \lesssim 5$ GeV can be included and secondly since the VDM picture allows for quantitative predictions of the Q^2- and to some extent also of the W-dependence of σ^{tot} while topological properties are only implied.

We first look into the Q^2 dependence. Fig. 16 shows (a) the prediction of the EVDM[24], of a similar approach by Etim and Masso[25] (EM) who replace the EVDM sum $\sum_n \Gamma_n V_n$ (see eq. (5)) by a different parametrization of the measured e^+e^- annihilation cross section, and a prediction by Alexander, Maor and Milstene[26] (AMM) who infer $\sigma(\gamma_V(Q^2), \gamma(P^2=0))$ from data on $\sigma(\gamma_V(Q^2),p)$, $\sigma(\gamma(P^2=0),p)$ and $\sigma(pp)$, basically using the relation $\sigma(\gamma_V(Q^2),\gamma) = \sigma(\gamma_V(Q^2),p) \cdot \sigma(\gamma,p)/\sigma(p,p)$ with appropriate kinematic threshold factors. It is obvious that all these hadronic approaches to the photon fail to describe the Q^2 dependence of $\sigma(\gamma_V(Q^2),\gamma)$ when averaged from W = 3 to 10 GeV. In Fig. 16b the same data is shown together with the Q^2 dependence of GVDM[10] and the absolute prediction by the QPM[3]. The GVDM cross section here is normalized to the data where it dominates clearly over the QPM prediction, at $W_{vis} > 4$ GeV, $\cos\theta^*(\gamma, \text{Jet}) > 0.9$, and $Q^2 < 1$ GeV^2. The GVDM cross section takes the form

$$\sigma^{GVDM}(W,Q^2) = \sigma_o \cdot F^{GVDM}(Q^2) \qquad (21)$$

with σ_o = 232 nb as average for $3 < W > 10$ GeV

It is obvious that the GVDM prediction falls below the data the more Q^2 increases. On the other hand the QPM prediction fails badly at low Q^2 ($Q^2 \lesssim 15$ GeV^2). We note that the sum of QPM and GVDM happens to coincide with the data at $0.1 < Q^2 < 100$ GeV^2.

The W dependence is investigated in Fig. 17. The AMM[26] prediction, at Q^2 = 0.44 GeV^2 (Fig. 17a) may be consistent with the data in the full W range, however at Q^2 = 5.4 GeV^2 (Fig. 17b) EVDM is clearly below the data at W > 4 GeV, while the AMM prediction is too low at all W > 2 GeV. In Fig. 18 the sum QPM + GVDM is compared to the PLUTO single-tag data. Since the GVDM does not really predict the W dependence of $\sigma_{\gamma\gamma}$, we chose the ansatz of eq. (21) with σ(W) = 232nb instead of σ_o. This sum also describes the W dependence at all three Q^2 regions. It thus turns out that the combination of the point-like picture in the QPM approximation with a specific hadronic picture of the photon describes the dependence over a large Q^2 region with a substantial variation of the cross section, and the W dependence of the total cross section.

Fig. 18b,c show also the cross section calculated thru eq. (1) from the following ansatz[27] for F_2 of the photon:

$$F_2(x, Q^2) = F_2^{QCD}(x, Q^2) + F_2^{VDM}(x, Q^2) \qquad (22)$$

where $F_2^{VDM} = 0.2 \cdot \alpha(1-x)$ is the structure function of the hadronic component of the target photon only:
Using the - singularity free - leading order QCD (LOQCD) prediction[28] for F_2^{QCD}, with Λ = 200 MeV, we get from eq. (1) the curves shown in Fig. 18b,c for Q^2 = 5.4 and Q^2 = 45 GeV^2. They are consistent with the data. For a discussion of other QCD predictions we refer to the talks by Bardeen[1] and Wagner[2].

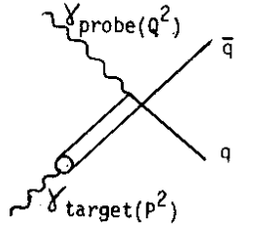

7. Summary and conclusions

- The total cross section, $\sigma^{tot}(\gamma\gamma \to \text{hadrons})$ has been measured in no-tag ($Q^2 = P^2 - 0$), single-tag ($0.1 < Q^2 < 100$ GeV^2) and double-tag ($0.1 \leq P^2$, $Q^2 \leq 1.6$ GeV^2) experiments, in the W range from 2 to 10 (20 for double-tag) GeV.
- A decomposition like $\sigma = A + \frac{B}{W} + \frac{C}{W^2}$ is unreliable for the present no-tag and single-tag data. There is no need for B, C terms at $Q^2 > 1$ GeV^2, nor in the double-tag data.
- The cross section factorization $\sigma(W,Q^2,P^2) = \sigma(W) \cdot F(Q^2) \cdot F(P^2)$ fails to link single-tag data at low ($\langle Q^2 \rangle = 0.44$) and high Q^2 ($\langle Q^2 \rangle = 5.4, 45$ GeV^2), and also the present single- and double-tag data both at low Q^2 (Q^2, $P^2 \lesssim 1.5$ GeV^2).
- "Hadronic" models which allow to describe $e^+e^- \to$ hadrons and ep scattering fail to describe the full Q^2 dependence in $\gamma\gamma$ scattering.
- The point-like predictions in the QPM approximation which work on average in e^+e^- annihilation at all s fail badly in $\gamma\gamma$ scattering at $Q^2 \leq 10$ GeV^2. Gluonic corrections are obviously much more important in $\gamma\gamma \to$ hadrons than in $e^+e^- \to$ hadrons.
- In contrast to $e^+e^- \to$ hadrons, where the sum QPM + GVDM amounts to double counting, the reaction $\gamma\gamma \to$ hadrons is well described by this sum in a large range of Q^2.
- $\sigma(W, Q^2)$ from $F_2^\gamma = F_2^{LOQCD} + F_2^{VDM}$ is also consistent with the data for $Q^2 > 1$ GeV^2, with $\Lambda \sim 200$ MeV.

Acknowledgement

I am grateful to numerous colleagues in the PLUTO and PEP4/9 collaborations. In particular I appreciate discussions with and support in providing results from Gideon Alexander, Alan M. Eisner, Barry King, Birgit Lewendel and Joachim Meyer. The organizers, the secretaries and the UC-Davis crew did a great job to make such a pleasant and fruitful meeting possible.

References

1) W.A. Bardeen, talk given at this workshop
2) W. Wagner, talk given at this workshop
3) V.M. Budnev et al., Phys. Rep. 15C (1975) 181, Yad.Phys. 13 (1971) 353
4) G. Rossi UCSD-10P10-227, Ph.D. thesis and UCSB-TH-83-01
5) PLUTO-Collaboration, Ch. Berger et al., Phys. Lett. 99B (1981) 287
6) J.L. Rosner, Brookhaven report CRISP 7126 (1971)
7) E. Witten, Nucl. Phys. B120 (1977) 189
W.A. Bardeen, A.J. Buras, Phys. Rev. D20 (1979) 166
D.W. Duke, J.F. Owens, Phys. Rev. D22 (1980) 2280
8) J.J. Sakurai, Phys. Lett. 46B (1973) 207
9) J.D. Bjorken and E.A. Paschos, Phys. Rev. 185 (1969) 1975
10) J.J. Sakurai and D. Schildknecht, Phys. Lett. 40B (1972) 121
I.F. Ginzburg and V.G. Serbo, Phys. Lett. 109B (1982) 231
11) M. Greco, Nucl. Phys. B63 (1973) 398
12) Proc. of the Fifth Int. Workshop on Photon Photon Collisions, Aachen 1983, ed. Ch. Berger, Springer Verlag (1983)
13) PEP-9 Two-Photon Collaboration, J.C. Armitage et al., Measurement of the Hadronic Photon-Photon Cross-Section in a Doubly-Tagged Experiment, Contribution to the XXII International Conference on High Energy Physics, Leipzig (1984), and presented at the parallel sessions of this workshop by D. Bintinger.
14) PLUTO-Collaboration, Ch. Berger et al., DESY 84-080, Measurement of the Total Photon-Photon Cross Section for the Production of Hadrons at Small Q^2, and Phys. Lett. 149B (1984) 421
B. Lewendel, Ph.D. Thesis, DESY PLUTO-84-o5, unpublished
15) PLUTO-Collaboration, Ch. Berger et al., DESY 84-081, A Measurement of the Q^2 and W Dependence of the $\gamma\gamma$ Total Cross Section for Hadron Production, and Z. Phys. 26C (1984) 353
16) PLUTO-Collaboration, in preparation
17) TASSO-Collaboration, R. Brandelik et al., Phys. Lett. 89B (1980) 418
TASSO-Collaboration, M. Althoff et al., DESY 83-130 (1983) and Z. Phys. C - Particles and Fields (to be published).
JADE-Collaboration, W. Bartel et al., Z. Phys. C - Particles and Fields 20 (1983) 187
PLUTO-Collaboration, Ch. Berger et al., Phys. Lett. 95B (1980) 313

C. Bacci et al., Phys. Lett. 86B (1979) 234 (ADONE)

J.L. Siegrist, Ph. D. Thesis SLAC-225 (1980) (MARK II)

M.S. Alam et al., Phys. Rev. Lett. 49 (1982) 357 (CLEO)

LENA-Collaboration, B. Niczyporuk et al., Z. Phys. C - Particle and Fields 9 (1981) 1

18) PLUTO-Collaboration, Ch. Berger et al., Z. Phys. C 26 (1984) 199

19) V. Blobel, Proceedings of the 1984 CERN school of computing, Aiguablava, September 1984,(to be published)

20) A. Bäcker, Talk given at this workshop

21) J.L. Rosner, BNL report 17552 (1972) 316
T.F. Walsh, J. Physique C2 Suppl. 3 (1974) 77

22) JADE-Collaboration, W. Bartel et al., Phys. Lett. 107B (1981) 163
PLUTO-Collaboration, Ch. Berger et al., Z. Phys. C26 (1984) 191

23) F. Foster talk given at this workshop
PLUTO-Collaboration, presented at the parallel sessions of this workshop by D. Schmidt

24) U. Maor and E. Gotsman, Phys. Rev. D28 (1983) 2149
and U. Maor, private communication

25) E. Etim and E. Masso, Z. Phys. C18 (1983) 117

26) G. Alexander, U. Maor and C. Milstene, Phys. Lett. 131B (1983) 224.

27) C. Peterson, T.F. Walsh, P.M. Zerwas, Nucl. Phys. B174 (1980) 424

28) E. Witten, ref. 7.

DISCUSSION

David O. Caldwell, U.C. Santa Barbara

QUESTION: I have one comment and one question. The comment is a correction to your introduction, in which the $Q^2 = 0$ γ-p total cross section was said to be explainable completely by VDM. In fact, the Santa Barbara measurements of the total cross sections for real photons from hydrogen and heavier nuclei gave the very first evidence for a point-like photon interaction. A consistent analysis of the magnitude of $\sigma_T(\gamma p)$ and of the A-dependence of $\sigma_T(\gamma A)$ required a point-like interaction, as well as VDM.

The question concerns the use of a sum of GVDM and QPM contributions to explain the $\gamma\gamma$ total cross section. Since the parameters of the GVDM model are chosen to fit deep inelastic e-p scattering, which surely has important parton contributions, is there not double counting in using a sum of GVDM and QPM?

ANSWER: I thank you very much for your comment - I simply was not aware of the analysis that you mention.

As to your question which addresses a central issue of my talk. The GVDM "predicts" the Q^2 dependence of reactions induced by photons with variable virtuality, by means of 8 parameters adjusted to fit ep scattering and e^+e^- annihilation. And this prediction should - as you state correctly - include parton contributions.

The absolute $\gamma\gamma$ cross section, however, is not really predicted. The absolute (GVDM-) cross section used here describes this data in a kinematic region (at the low Q^2 end, see sect. 6.3) where the QPM contribution is down to a few percent of the measured total. Here the GVDM normalization is anchored. Therefore, the GVDM part is not underestimated. With this correct or consistent normalization the GVDM part is lower than the data at large Q^2 (see Fig. 16). The excessive cross section at large Q^2 is - that is my understanding - due to the point-like (QED) coupling of the target photon to partons, as calculated by the QPM. The GVDM part is responsible for the hadron-like coupling (thru ρ, ω, ϕ ...) of the target photon to partons,

which of course interact with the probe photon (at large Q^2) as incoherent partons. At low Q^2, the probe photon acts as vector meson, mainly. To the extent that QPM does not 'contain' VDM-like γ-hadron transitions for the target photon, I think there is no double counting in the sum of GVDM and QPM. The data seem to say: the sum of QPM and GVDM is neither too low, i.e. is sufficient, nor too high, i.e. no double-counting.

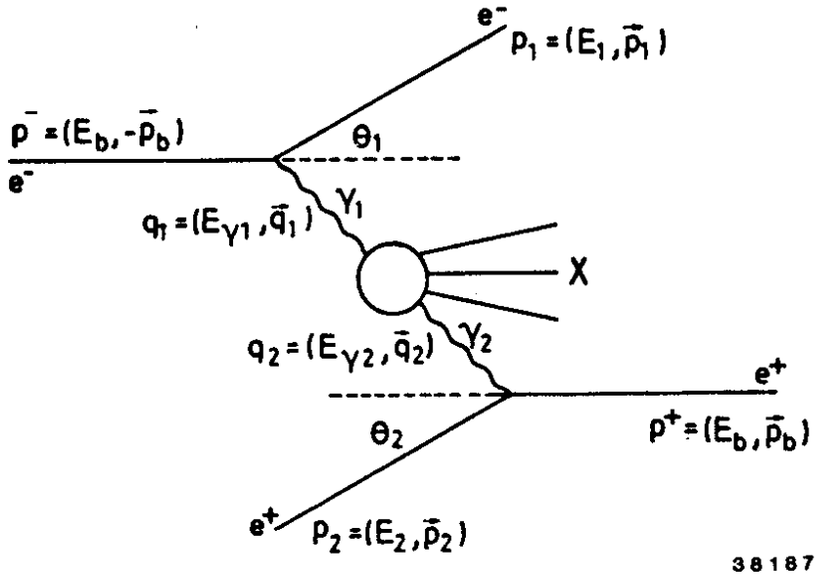

Fig. 1: Definition of variables for the reaction $e^+e^- \to e^+e^- + X$

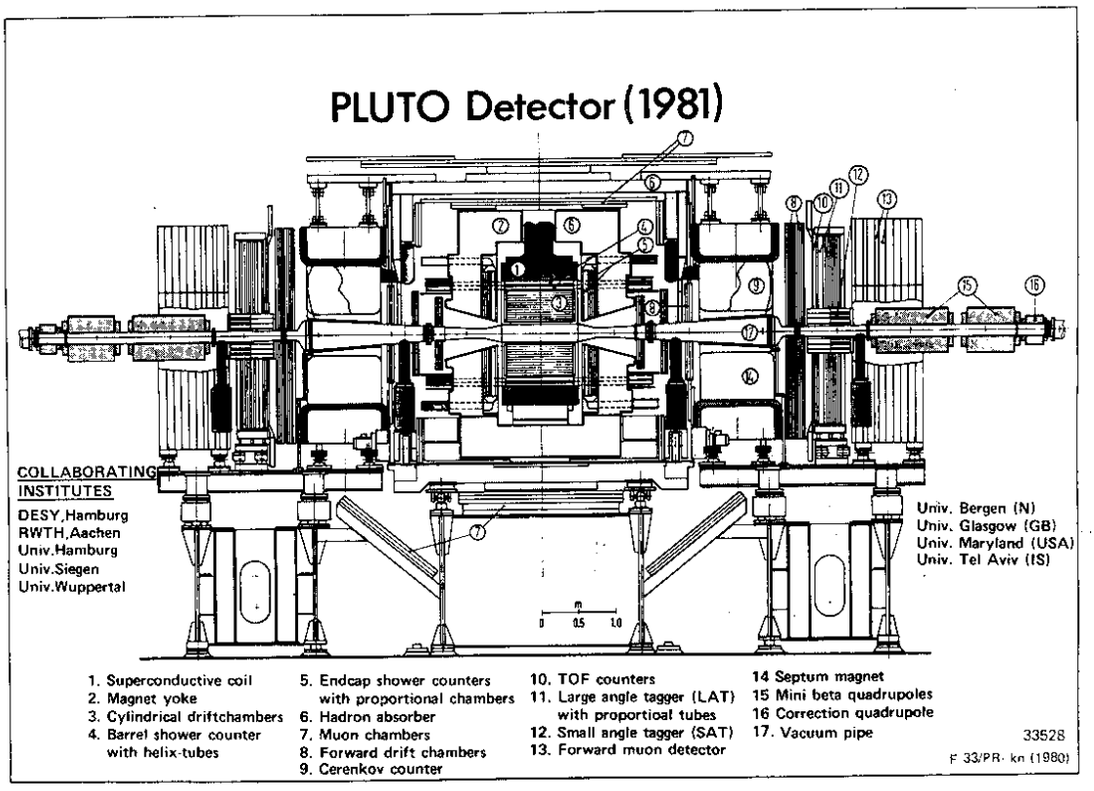

Fig. 2a

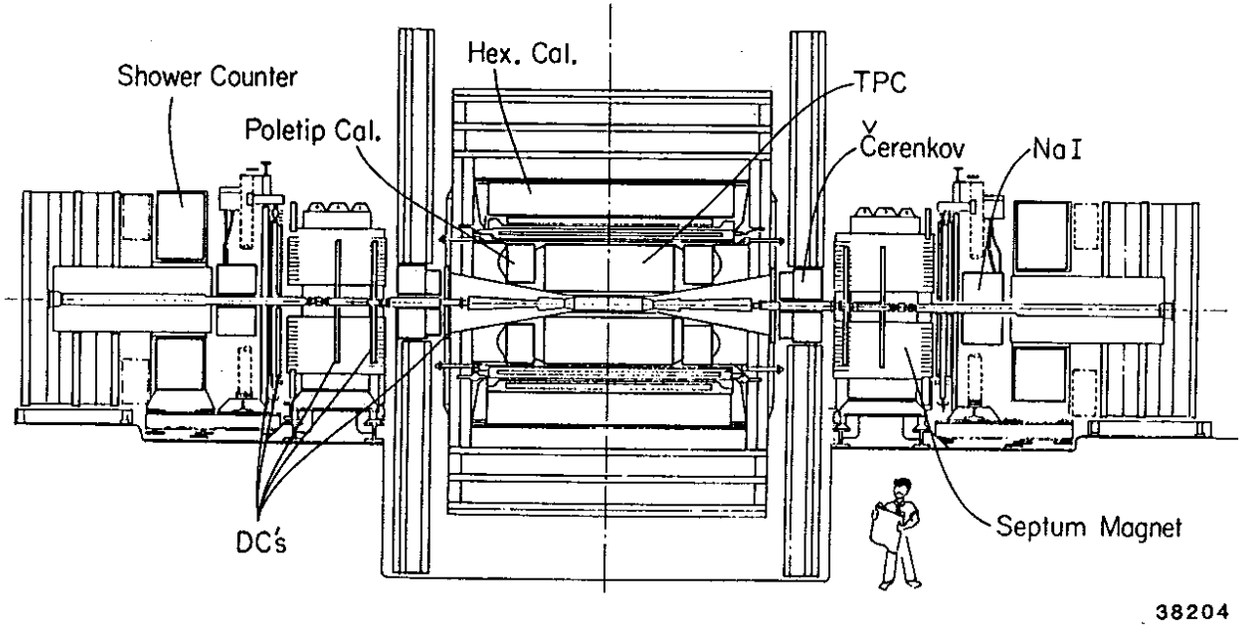
Shower Counter
Poletip Cal.
Hex. Cal.
TPC
Cerenkov
NaI
DC's
Septum Magnet
38204

Fig. 2b

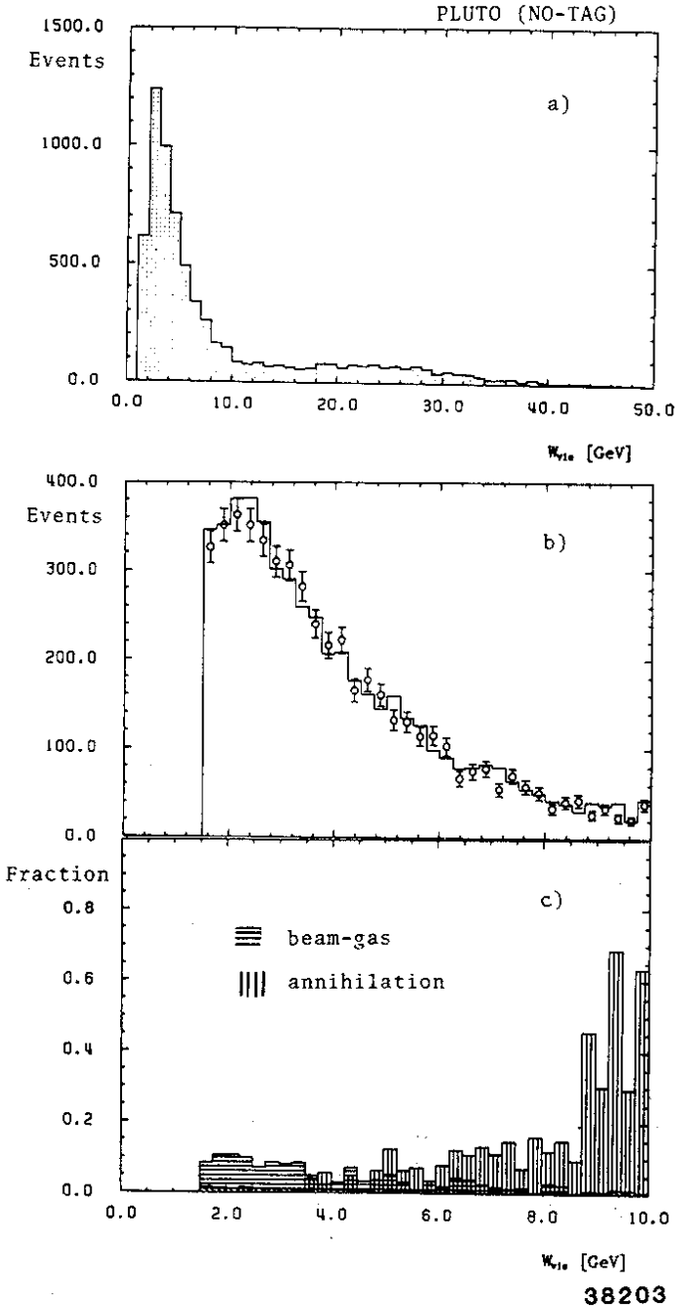

Fig. 3: No-tag event distributions: (a) all W_{vis}, data, (b) $W_{vis} <$ 10 GeV, data as circles, MC simulation including background as histogram, (c) estimated background as fraction of the observed sample, from e^+e^- annihilation (vertical lines), from beam gas (horizontal lines), and from $\gamma\gamma \to \tau\tau$ (skew lines).

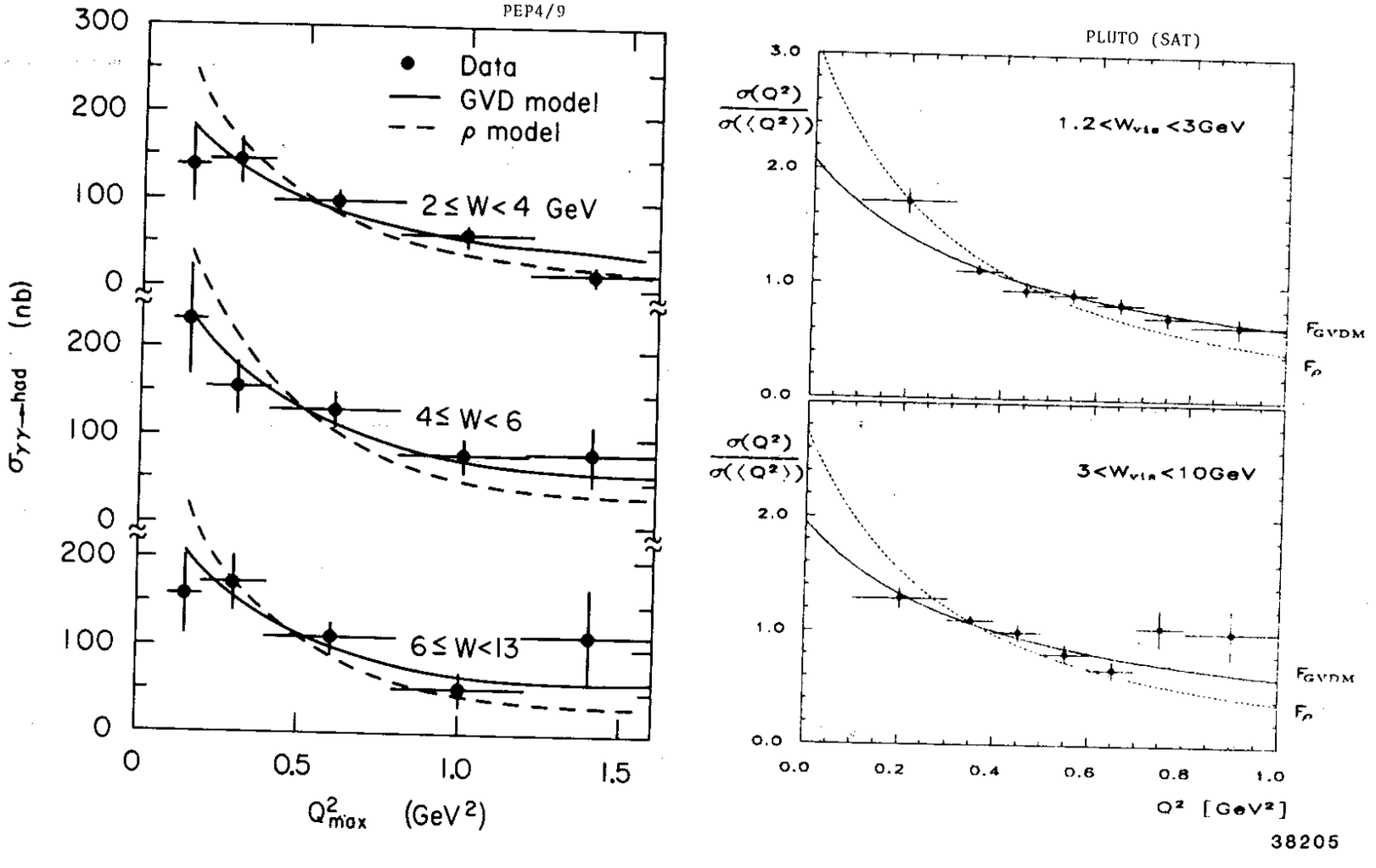

Fig. 4: Q^2 distributions from double-tagging (the larger Q^2 value) and from single-tagging data, for several W_{vis} intervals, in comparison with GVDM and ρ-pol form factor.

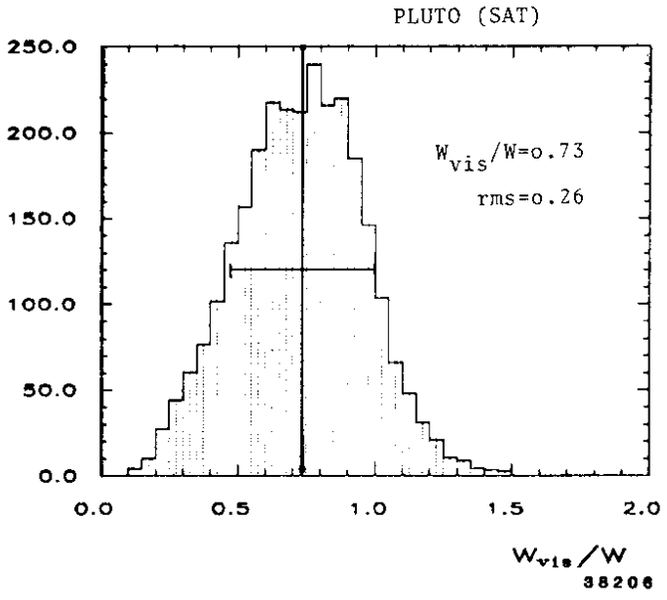

Fig. 5:

The W_{vis} resolution (W_{vis}/W) for PLUTO SAT from MC simulation.

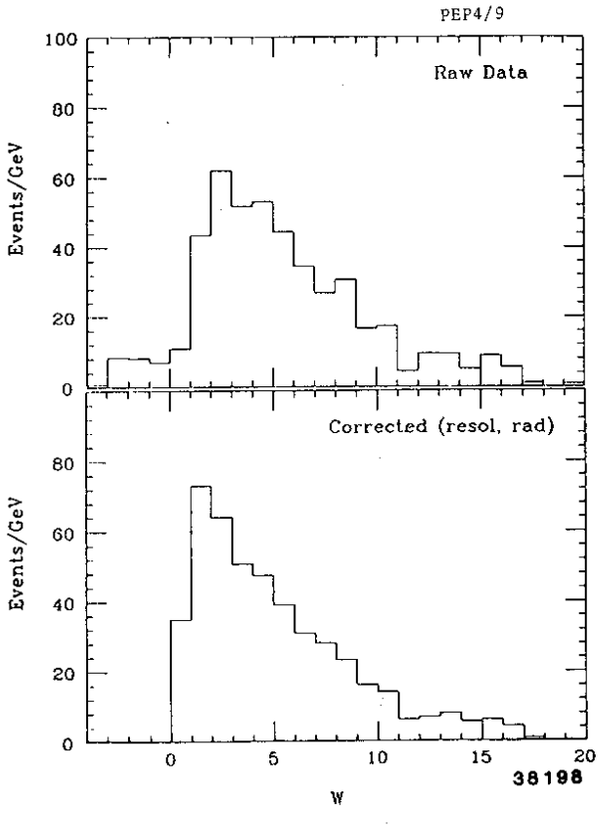

Fig. 6:

The W distribution from PEP4/9 double-tagging data: as measured, and after correction for resolution and radiative effects.

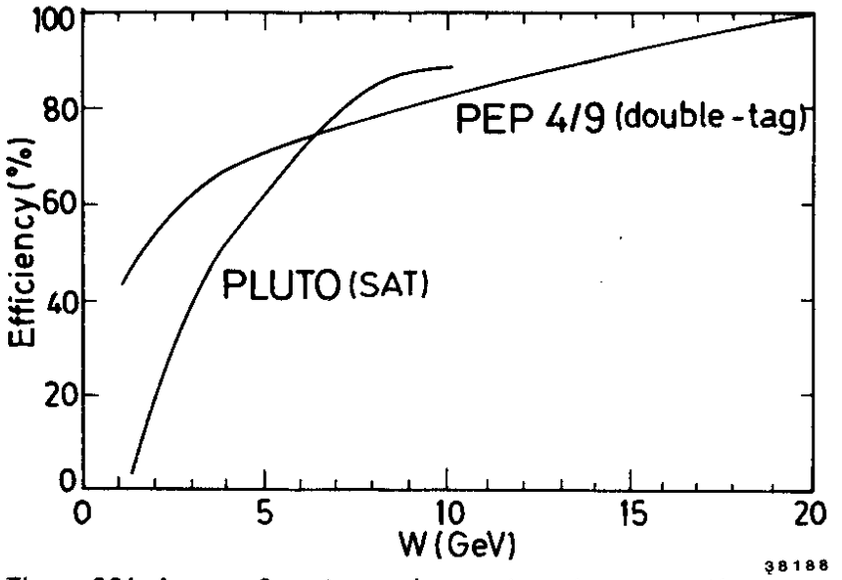

Fig. 7: The efficiency for tagged events to pass the event selection criteria, as function of W, for PEP4/9 and PLUTO(SAT).

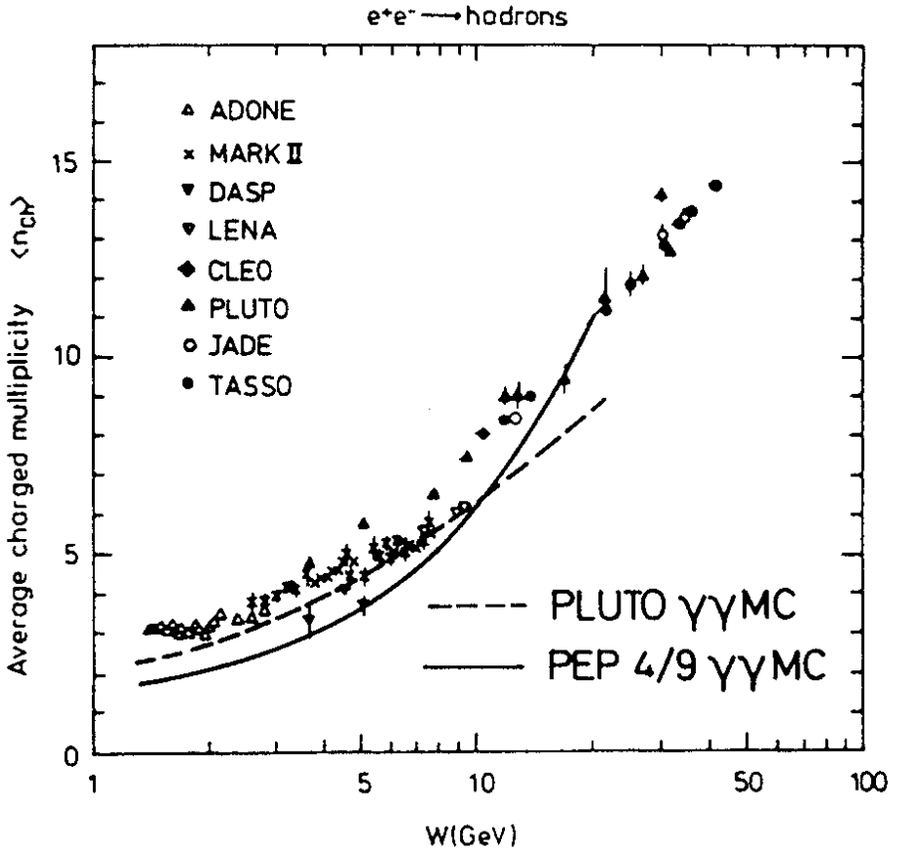

Fig. 8a: Average charged multiplicity. Data points from e^+e^- annihilation. Curves show $\langle n_{ch} \rangle$ as used in the PEP4/9 and PLUTO $\gamma\gamma \rightarrow$ hadrons simulations.

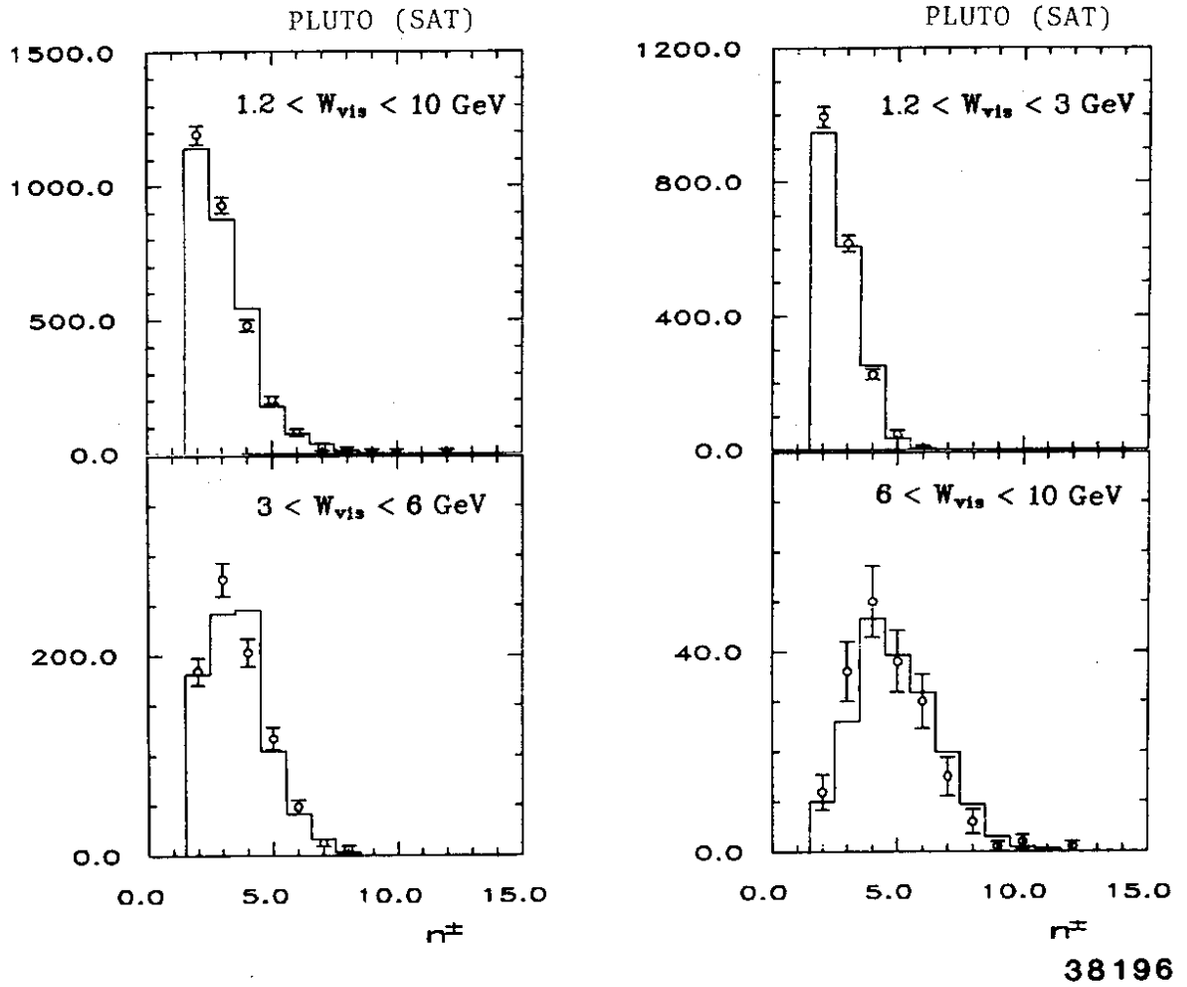

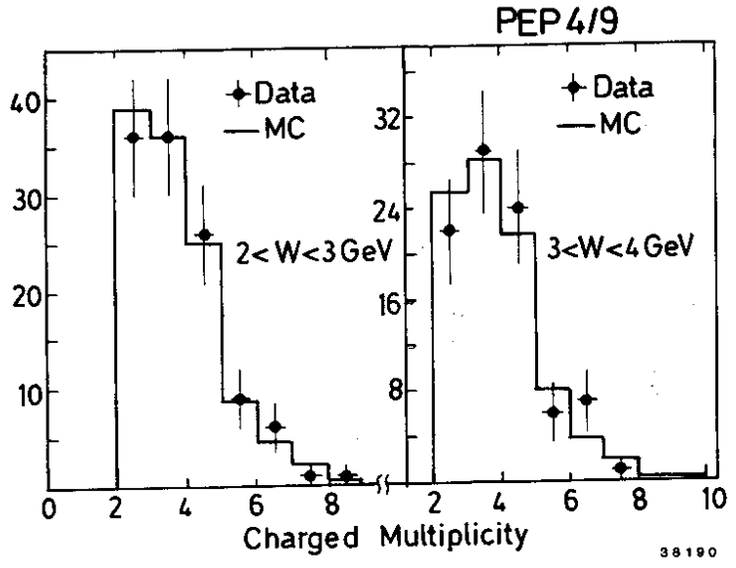

Fig. 8b: Charged particle multiplicity distribution in selected W_{vis} regions, from PLUTO (SAT) and PEP4/9 double-tagging, data (circles) and MC simulation (histogram).

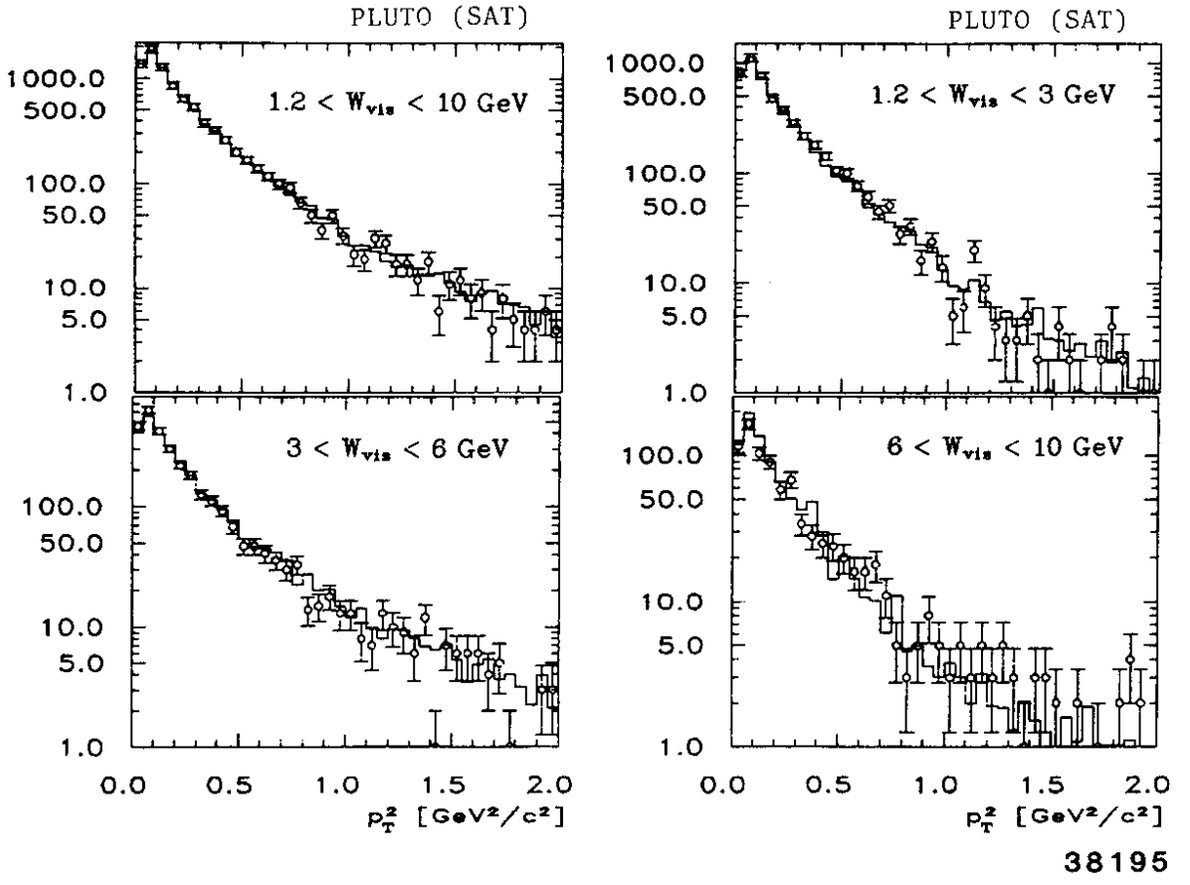

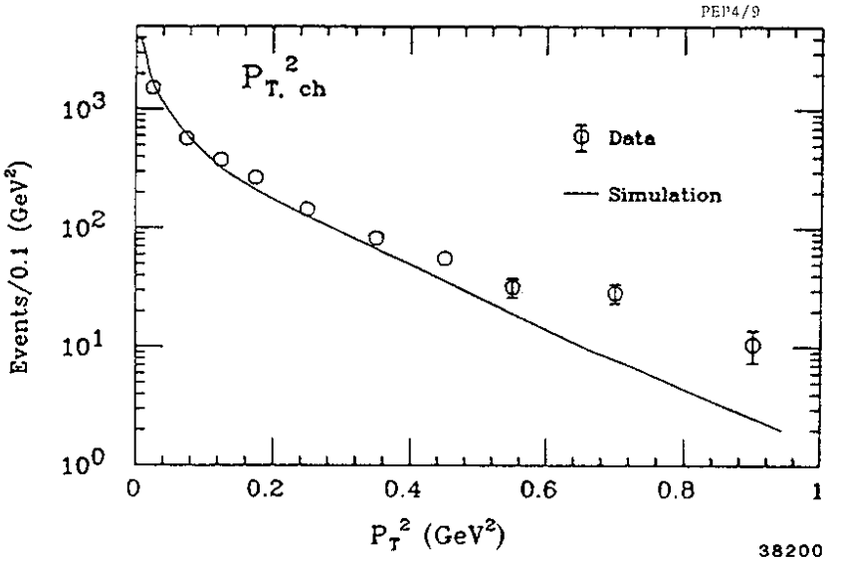

Fig. 9: Charged particle $P_\perp^2$ (w.r.t. beam) distribution from PLUTO (SAT) and PEP 4/9 double-tagging, data (circles) and MC simulation (histogram, curve).

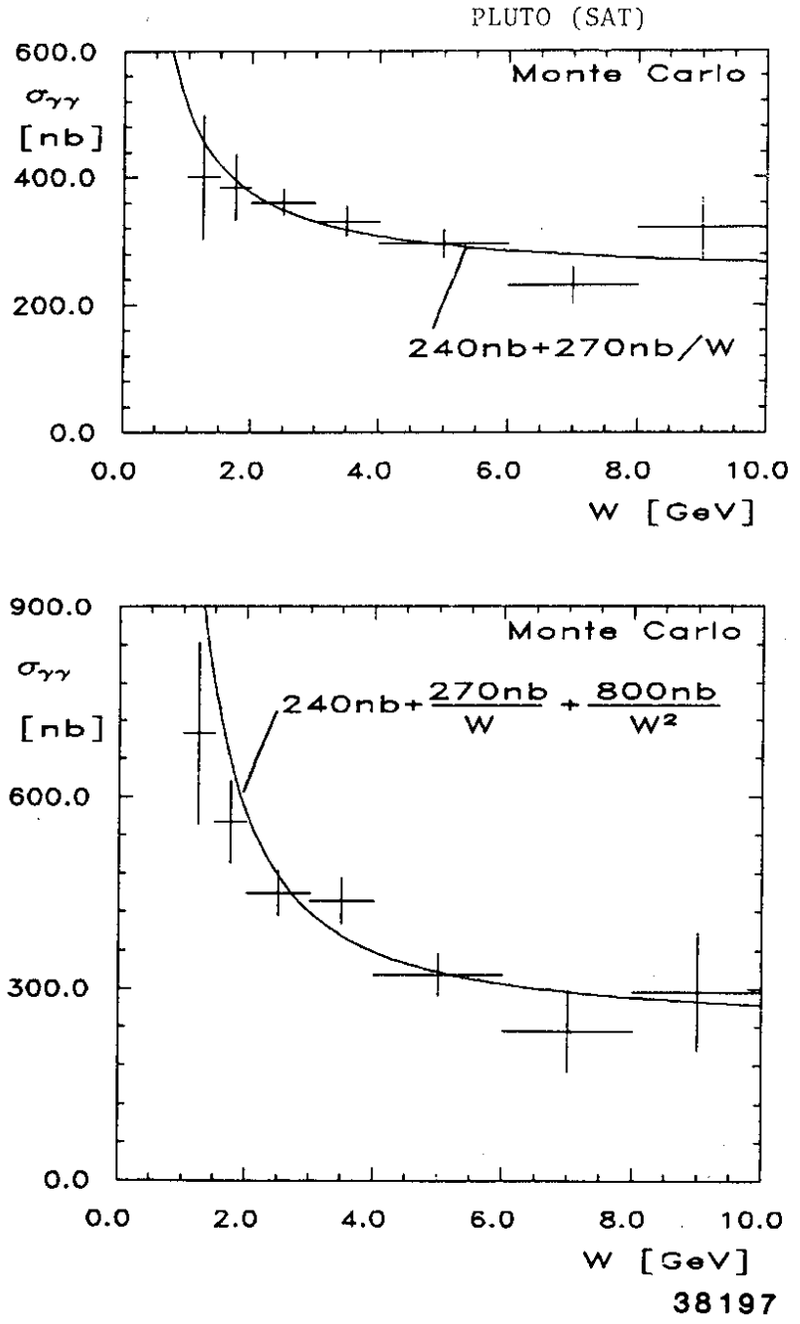

Fig. 10: Test of the unfolding procedure. The curves are the input cross section for simulated experiments (PLUTO-SAT), and the crosses are the results from the analysis.

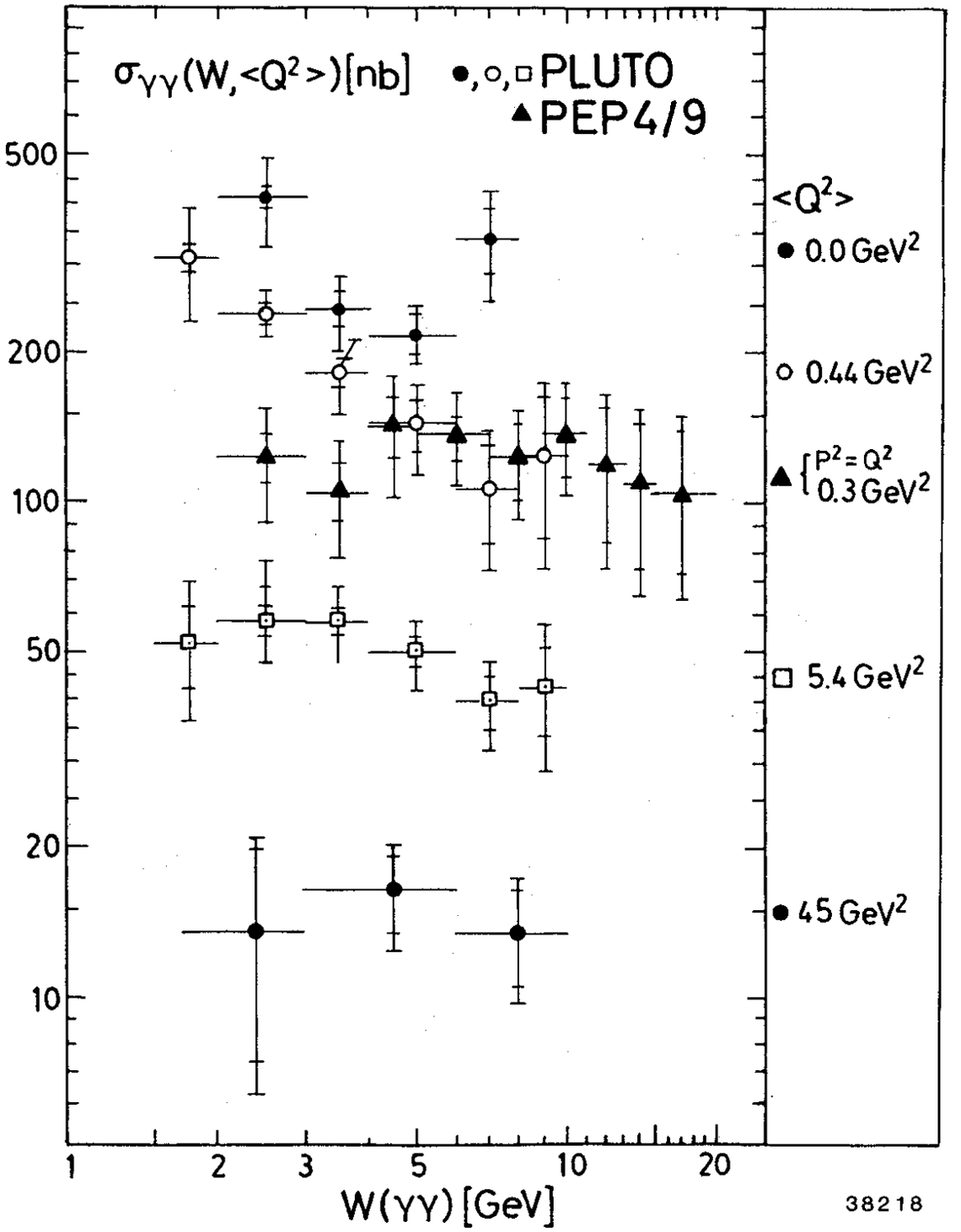

Fig. 11: The cross section $\sigma_{\gamma\gamma}$ (W, $<Q^2>$, $<P^2>$) for no-tagging, single-tagging and double-tagging measurements. All PLUTO data are at $<P^2>$ = 0.01 GeV^2. The double-tag data in the region 5<W<11 GeV, originally presented in 1 GeV bins (see Fig. 15), have been rebinned here by the author into 2 GeV bins.

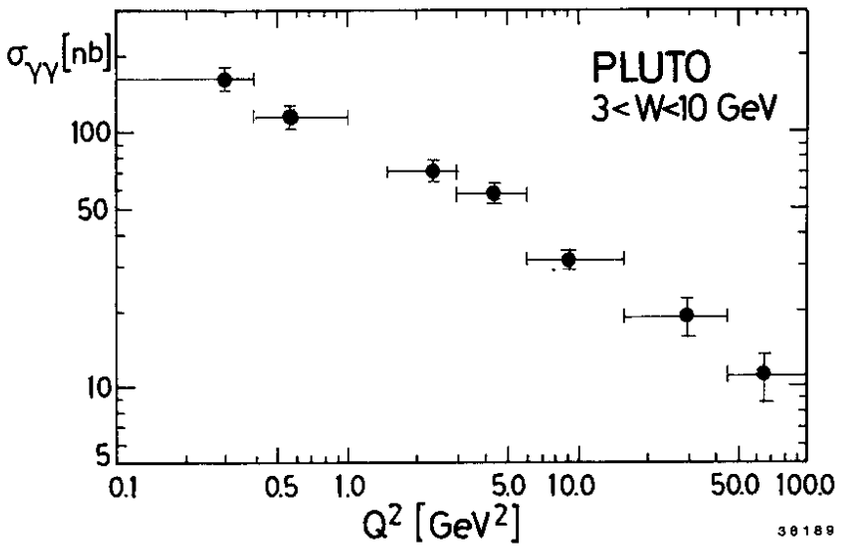

Fig. 12: The Q^2 dependence of $\sigma_{\gamma\gamma}$, averaged over $3 < W < 10$ GeV, from the PLUTO single-tagging data.

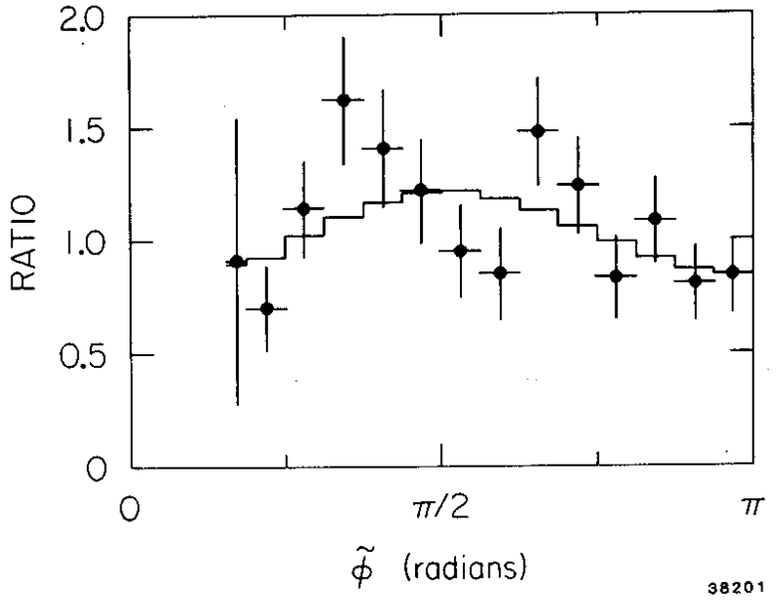

Fig. 13: Ratio of σ_{eff} plus interference terms (τ) to σ_{eff} vs. acoplanarity $\tilde{\phi}$ in $\gamma^*\gamma^*$ center of mass, for $W > 2$ GeV. The histogram is the best fit for σ_{eff}, τ_{TT} and τ_{TL} in eq. (9).

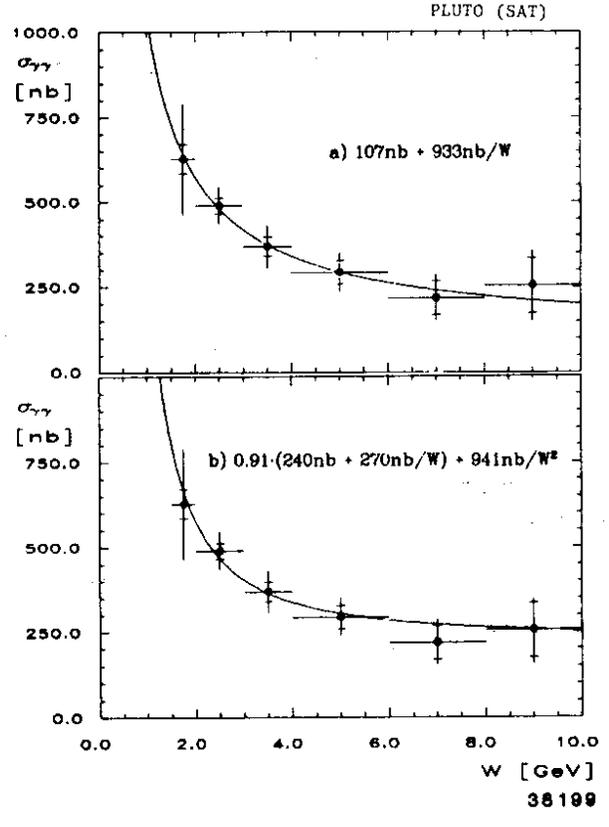

Fig. 14: Fits of power terms to $\sigma(W)$: (a) with a W^0 and W^{-1}, (b) the traditional (ref. 21) VDM estimate and a W^{-2} term.

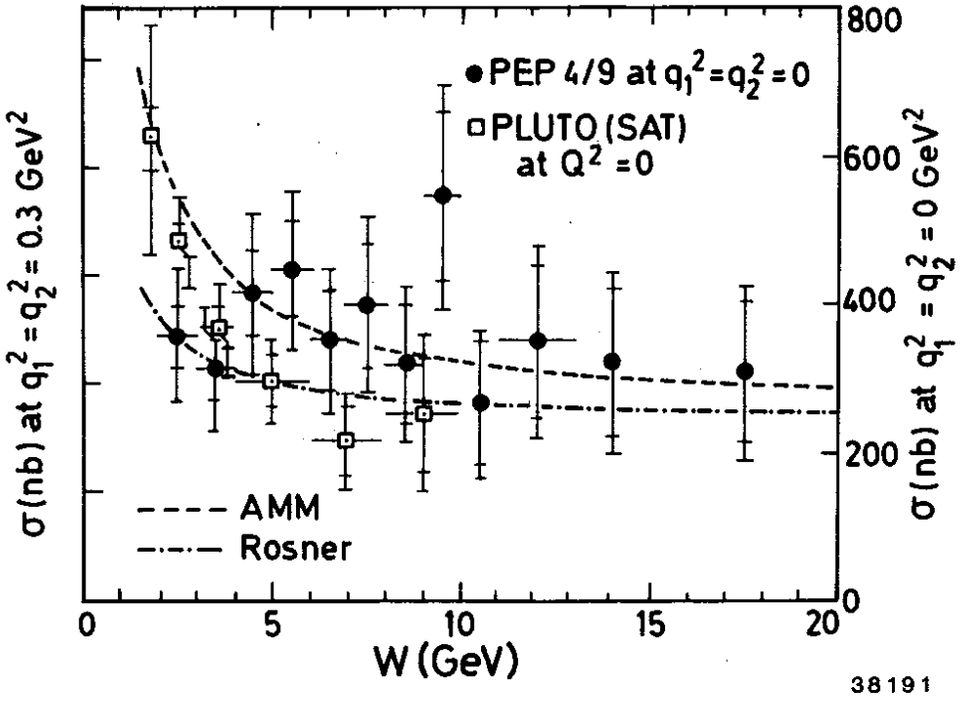

Fig. 15: The PEP4/9 double-tagging and the PLUTO-SAT cross section extrapolated to $P^2 = Q^2 = 0$, using GVDM form factors, in comparison with the old (Rosner, ref. 21) and the improved (AMM, ref. 26) VDM predictions.

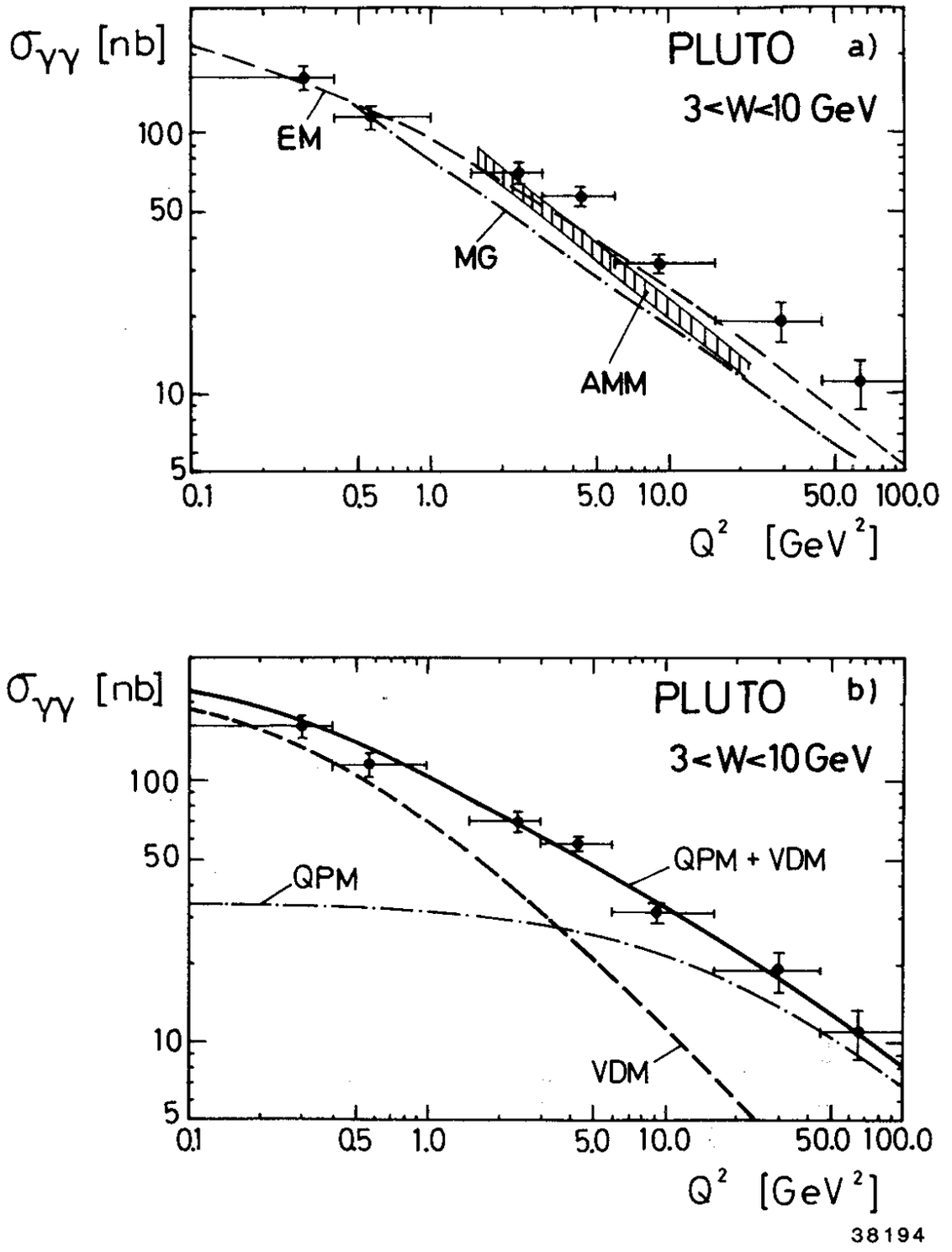

Fig. 16: The Q^2 dependence of $\sigma_{\gamma\gamma}^{tot}$, for $3 < W < 10$. The PLUTO data are compared (a) to two versions of EVDM (by Etim and Masso[25]) (EM) and by Maor and Gotsman[24]) (MG)) and to the factorization approach by Alexander et al.[26]) (AMM); and (b) to a GVDM prediction (VDM, see text eq. (19)) and the QPM prediction.

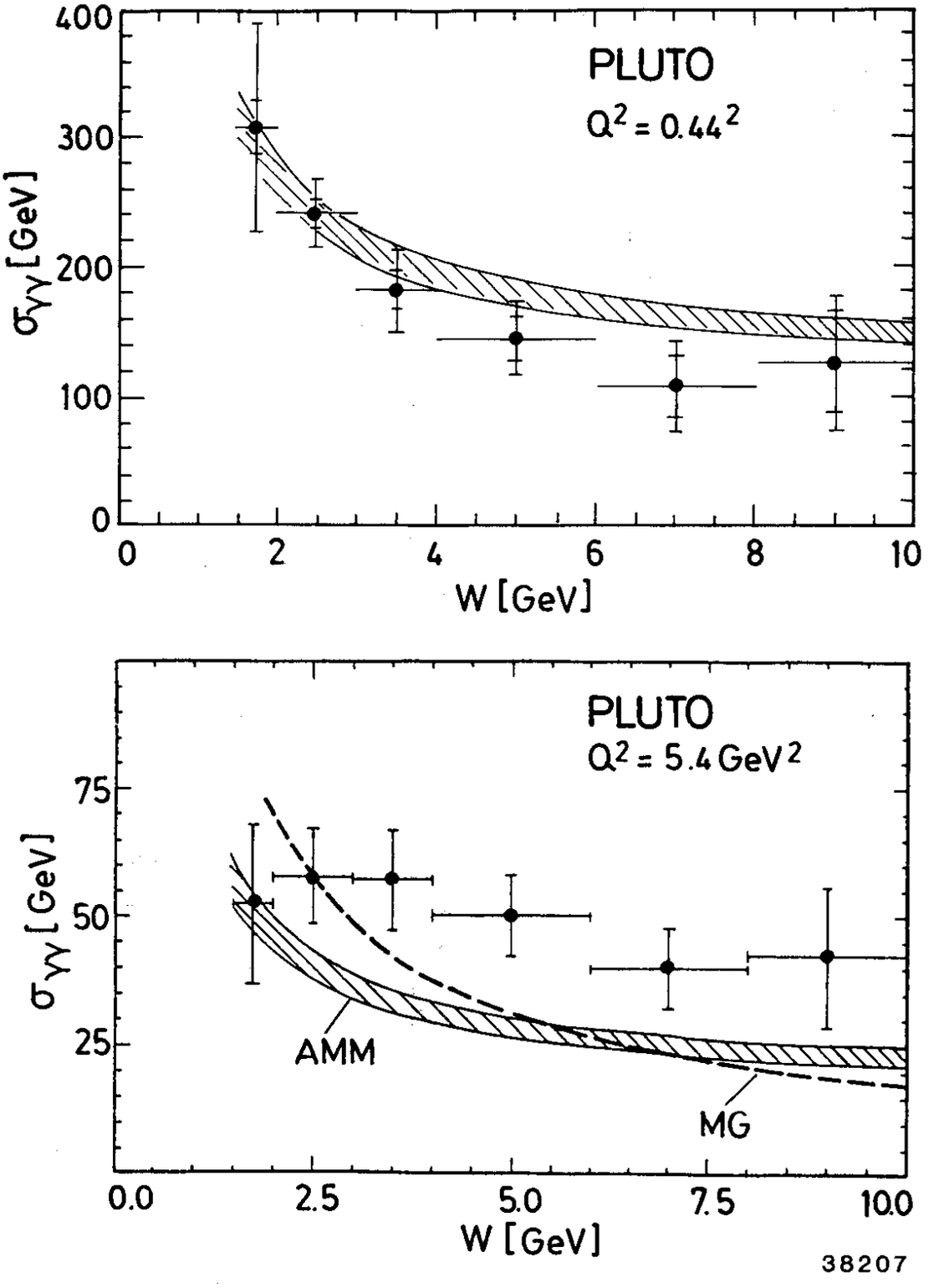

Fig. 17: The W dependence of $\sigma_{\gamma\gamma}^{tot}$, (a) at $\langle Q^2 \rangle = 0.44$ GeV^2 and (b) at $\langle Q^2 \rangle = 5.4$ GeV^2. The curves are explained in Fig. 16.

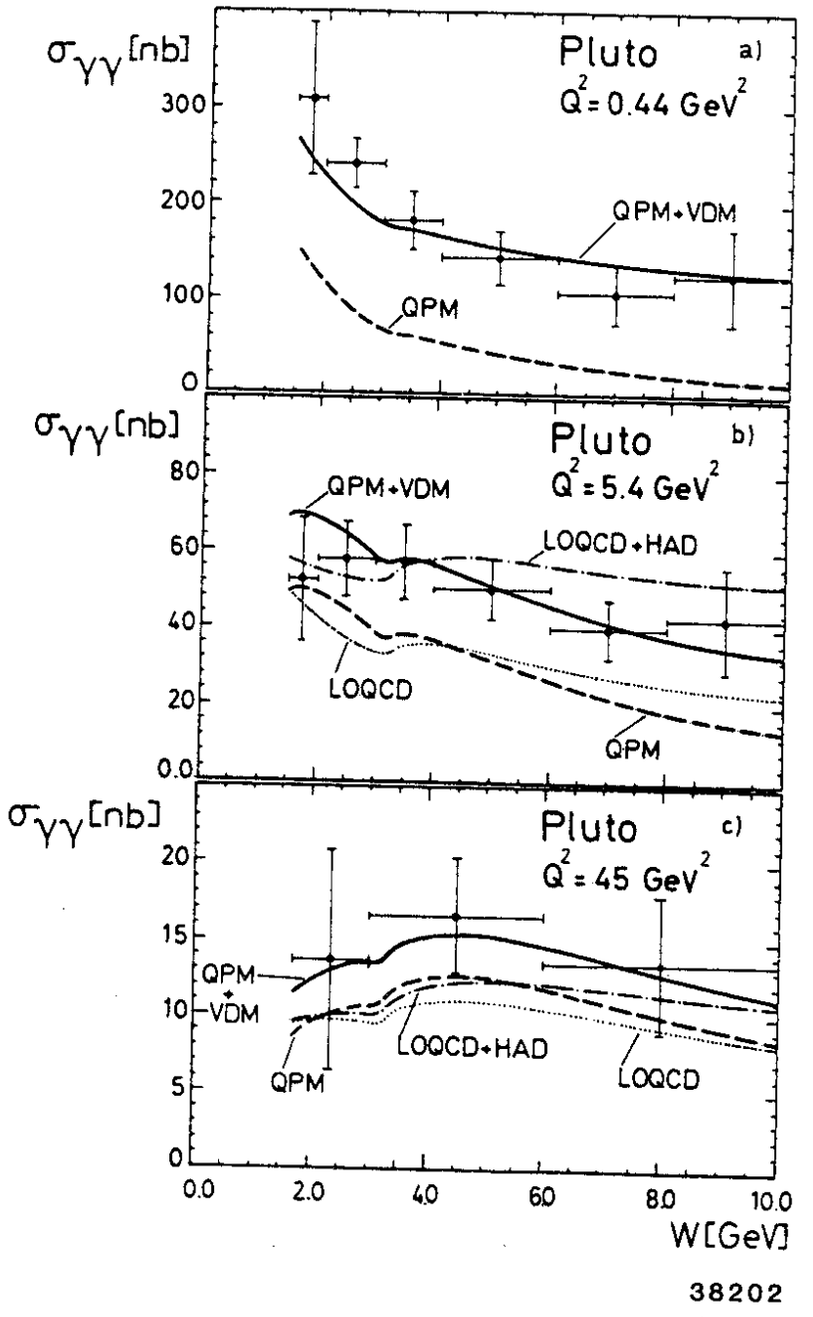

Fig. 18: The W dependence of $\sigma_{\gamma\gamma}^{tot}$ at $\langle Q^2 \rangle$ = 0.44, 5.4 and 45 GeV^2. The curves labeled QPM and QPM + VDM are defined in Fig. 16, the one labeled LOQCD is from the leading order QCD prediction[27] for F_2^γ, with Λ = 200 MeV, and LOQCD + HAD includes a hadronic component, $F_2^{had} = \alpha \cdot 0.2(1-x)$.